

QUASI-QUIESCENT RADIO EMISSION FROM THE FIRST RADIO-EMITTING T DWARF

PETER K. G. WILLIAMS¹, EDO BERGER¹, AND B. ASHLEY ZAUDERER¹

Submitted ApJL 2013 Jan 10; revised 2013 Mar 12; accepted 2013 Mar 13

ABSTRACT

Radio detections of ultracool dwarfs provide insight into their magnetic fields and the dynamos that maintain them, especially at the very bottom of the main sequence, where other activity indicators dramatically weaken. Until recently, radio emission was only detected in the M and L dwarf regimes, but this has changed with the Arecibo detection of rapid polarized flares from the T6.5 dwarf 2MASS J10475385+2124234. Here, we report the detection of quasi-quiet radio emission from this source at 5.8 GHz using the Karl G. Jansky Very Large Array. The spectral luminosity is $L_\nu = (2.2 \pm 0.7) \times 10^{12}$ erg s⁻¹ Hz⁻¹, a factor of ~ 100 times fainter than the Arecibo flares. Our detection is the lowest-luminosity yet achieved for an ultracool dwarf. Although the emission is fully consistent with being steady, unpolarized, and broadband, we find tantalizing hints for variability. We exclude the presence of short-duration flares as seen by Arecibo, although this is not unexpected given estimates of the duty cycle. Follow-up observations of this object will offer the potential to constrain its rotation period, electron density, and the strength and configuration of the magnetic field. Equally important, follow-up will address the question of whether the electron cyclotron maser instability, which is thought to produce the flares seen by Arecibo, also operates in the very different parameter regime of the emission we detect, or whether instead this ultracool dwarf exhibits both maser and gyrosynchrotron radiation, potentially originating from substantially different locations.

Subject headings: brown dwarfs — radio continuum: stars — stars: individual (2MASS J10475385+2124234)

1. INTRODUCTION

Although there is now abundant evidence that very low-mass stars and brown dwarfs (collectively, ultracool dwarfs: UCDs) can host significant magnetic activity, the origins and detailed nature of this activity are not well-understood. While there is consensus that the $\alpha\Omega$ dynamo that powers the solar magnetic field cannot operate in these fully-convective objects, modeling of turbulent dynamos yields a wide range of predictions for the strength, morphology, and time-dependence of UCD fields (e.g., Durney et al. 1993; Chabrier & Küker 2006; Dobler et al. 2006; Browning 2008). These poorly-constrained yet basic physical properties affect the internal structure, atmospheric conditions, and dynamics of low-mass stars, brown dwarfs, and giant planets.

The evidence for UCD magnetic activity comes from a variety of tracers. Standard indicators such as X-ray and H α emission (e.g., Rutledge et al. 2000; West et al. 2004) have been augmented by Zeeman-Doppler imaging (ZDI; Semel 1989; Donati et al. 2008; Morin et al. 2008) and FeH spectroscopy (Reiners & Basri 2006, 2007). A particularly noteworthy discovery was the detection of UCD radio emission (Berger et al. 2001), which is much stronger than would be expected from stellar scaling relations (Güdel & Benz 1993; Benz & Güdel 1994). Radio emission is an increasingly important observable because other tracers become much more difficult to exploit for the very latest-type dwarfs, in which rapid rotation obliterates Zeeman signals, the overall optical luminosity decreases greatly, and X-ray and H α emission fall off precipitously (Stelzer et al. 2006; Berger et al. 2010; Gizis et al. 2000; West

et al. 2004). This last effect is possibly due to increasingly neutral atmospheres (Mohanty et al. 2002), enhanced trapping of energetic electrons, centrifugal stripping of the corona, or other effects decreasing the efficiency with which the coronal plasma is heated (Berger et al. 2010).

A deeper understanding of the convective dynamo will likely be built upon a clearer picture of the magnetic phenomenology of UCDs across the widest possible range of temperatures and Rossby numbers. Measurements of activity in the latest dwarfs, which are extreme in both these parameters, are thus vital. Until recently, the latest-type UCD to be detected in the radio was the L3.5 object 2MASS J00361617+1821104 (Berger 2002; Berger et al. 2005; Hallinan et al. 2008). However, in the past year, two later-type sources have been detected. The L5e+T7 binary 2MASS J13153094-2649513AB (2M 1315–26 hereafter), known to have strong long-lived H α emission (Hall 2002; Burgasser et al. 2011), was shown by Burgasser et al. (2013) to have quiescent radio emission. Even more surprisingly, the T-dwarf barrier was broken by Route & Wolszczan (2012, RW12 hereafter), who detected circularly-polarized radio bursts from the T6.5 dwarf 2MASS J10475385+2124234 (2M 1047+21 hereafter) with the Arecibo observatory. At a distance of 10.6 pc and a temperature of a mere ~ 900 K (Vrba et al. 2004), 2M 1047+21 represents a new benchmark in the study of cool, magnetically-active objects.

In this Letter, we report the detection of 2M 1047+21 with the Karl G. Jansky Very Large Array (VLA) with properties significantly different from those of the flares detected by RW12 (§2). We discuss its implications as well as some potential paths forward (§3).

2. OBSERVATIONS & ANALYSIS

pwilliams@cfa.harvard.edu

¹Harvard-Smithsonian Center for Astrophysics, 60 Garden Street, Cambridge, MA 02138, USA

2M1047+21 was spectroscopically identified as a T dwarf by Burgasser *et al.* (1999). It was later assigned spectral types of T7 (optical; Burgasser *et al.* 2003a) and T6.5 (near infrared; Burgasser *et al.* 2006). Burgasser *et al.* (2003a) also made a marginal (2.2σ) detection of H α emission, measuring a flux of $f_{\text{H}\alpha} = (5.9 \pm 2.7) \times 10^{-18} \text{ erg cm}^{-2} \text{ s}^{-1}$. Astrometric monitoring revealed a distance of $10.6 \pm 0.4 \text{ pc}$ and a proper motion of $1728.4 \pm 7.7 \text{ mas yr}^{-1}$ (Vrba *et al.* 2004). Vrba *et al.* (2004) also computed a bolometric luminosity of $\ell_{\text{bol}} = -5.36$ for 2M1047+21, where $\ell = \log_{10}(L/L_{\odot})$. Combining these results, $\ell_{\text{H}\alpha} - \ell_{\text{bol}} = -5.3 \pm 0.2$, well above the trend for typical UCDs (Berger *et al.* 2010). There is no evidence for 2M1047+21 being a binary system, with Burgasser *et al.* (2003b) ruling out companions at separations $\gtrsim 4 \text{ AU}$ with mass ratios $\gtrsim 0.4$ and Carson *et al.* (2011) finding weaker constraints. Before the radio detection by RW12, Berger (2006) reported a flux density upper limit of $45 \mu\text{Jy}$ at 8.46 GHz ($\ell_r - \ell_{\text{bol}} < -5.52$, where $L_r = \nu L_{\nu}$)².

Using the astrometric parameters of Vrba *et al.* (2004), the predicted location of 2M1047+21 at the time of our VLA observations is RA = 10:47:52.03, Dec = +21:24:16.7 (FK5 J2000). We use a simple Monte Carlo approach to estimate the 1σ -confidence ellipse in this position to have major and minor axes of $0.19''$ and $0.09''$ at a position angle of 77° . This is much smaller than the $\sim 1''$ astrometric uncertainties of our observation in the VLA C configuration at $\sim 6 \text{ GHz}$ and much larger than the difference between the FK5 and ICRS frames.

We observed 2M1047+21 in a two-hour session starting on 2012 April 17.02 UT (project 12A-451). The total correlated bandwidth is 2048 MHz, with two basebands centered at 5000 and 6750 MHz and divided into 512 channels each. Standard calibration observations were obtained, using 3C 286 as the flux density standard and bandpass calibrator and the quasar J1051+2119 (0.9° from 2M1047+21) serving as the complex antenna gain calibrator. The total integration time on 2M1047+21 is 80 minutes. The data were calibrated using standard procedures in the CASA software system (McMullin *et al.* 2007). Radio frequency interference was flagged manually.

We created a deep Stokes I image of 2048×2048 pixels, each $1'' \times 1''$, using multi-frequency synthesis (Sault & Wieringa 1994) and CASA’s multifrequency CLEAN algorithm with two spectral Taylor series terms for each CLEAN component; this approach models both the flux and spectral index of each source. The synthesized beam is $4.2'' \times 3.6''$ and the reference frequency is 5.84 GHz, with data taken at frequencies between 4.51 and 7.24 GHz contributing to the imaging process. In the resulting image of the initial Taylor term (i.e., brightness at the reference frequency) we detect a 4.6σ (peak-to-rms) unresolved source at RA = 10:47:52.10, Dec = +21:24:16.2 (ICRS J2000) with 1σ positional uncertainties of $0.9''$ and $0.6''$ in RA and declination, respectively. The separation from the IR astrometric prediction is $1.0''$ at a position angle of 117° . Taking into account only the uncertainties on the VLA source position, and not the uncertainties in the IR position or the astrometric calibration of the VLA image, the separation is 1.3σ . The relevant portion of the image

is shown in Figure 1. Because we search for a source at only one *a priori* image position, the stringent detection criteria that have been advocated for blind radio source searches (e.g., Frail *et al.* 2012) do not apply.

Fitting the image region near the source with a Gaussian shaped like the synthesized beam, we find a flux density of $16.5 \pm 5.1 \mu\text{Jy}$ while the rms residual of the deconvolution process in the neighborhood is $3.6 \mu\text{Jy bm}^{-1}$, well above the $\sim 0.2 \mu\text{Jy bm}^{-1}$ confusion limit for this observing setup (Condon 2002). The uncertainty in the flux density is that reported by the fitting process, which is not generically equal to the background rms due to the two positional parameters. The overall significance of the peak, however, is set by the rms. We identify this source with 2M1047+21. The likelihood of a spurious association is small: Fomalont *et al.* (1991) found the density of radio sources brighter than $16 \mu\text{Jy}$ at 5 GHz to be $\sim 2 \times 10^{-4} \text{ arcsec}^{-2}$, making the probability of background source contamination $\sim 10^{-3}$ (assigning our search area to be the synthesized beam size). We counted peaks $> 16 \mu\text{Jy}$ in the central region of our image and found a density of $\sim 2.4 \times 10^{-4} \text{ arcsec}^{-2}$, agreeing well with the Fomalont *et al.* (1991) value. Our measurement does not account for primary beam attenuation, but the correction for that effect is a factor of a few, not large enough to change the conclusion of a low probability of chance coincidence.

The deconvolution process also determines a nominal spectral index of $\alpha = 0.9 \pm 1.0$ ($S_{\nu} \propto \nu^{\alpha}$). We also imaged the two VLA basebands separately with only one spectral Taylor term, i.e., assuming spectrally flat emission, and detected emission consistent with the position of 2M1047+21 in both images. The best-fit flux density of the source in the lower-frequency image is $18.0 \pm 9.2 \mu\text{Jy}$, larger than that in the higher-frequency image, $16.7 \pm 9.7 \mu\text{Jy}$; in both cases, the best-fit position is ~ 0.5 of a beam away from the best-fit position in the combined image. These fluxes tentatively suggest $\alpha < 0$, but the uncertainties are large. Combining our results with the upper limit of Berger (2006) at 8.46 GHz implies $\alpha \lesssim 2.7$ if variability is not a factor. Without calibrating the instrumental polarization leakages, we imaged the Stokes V parameter and found no emission at the location of 2M1047+21. We estimate $|V|/I \lesssim 80\%$ (3σ).

The radio emission detected by RW12 comprised flares with flux densities up to $\sim 2 \text{ mJy}$ on timescales of minutes. Thanks to the excellent sensitivity of the VLA, less than a second of integration time would be needed for a 5σ detection of these flares in our data, so superb time resolution of any flares should be possible. We searched for flares and other variability using a visibility-domain analysis. We subtracted the emission of all other detectable sources from the u - v data and summed the residual visibilities after rephasing to the position of 2M1047+21. Ignoring noise and calibration errors, the real part of the summed rephased visibility is the source flux, while the imaginary part is zero. Given that noise and calibration errors are always present, the variation of the imaginary part provides an assessment of the uncertainty in the real part. The mean real part is $16.5 \mu\text{Jy}$ and the variance associated with the imaginary parts $\sigma_{\text{im}}/\sqrt{N_{\text{im}}} = 4.6 \mu\text{Jy}$, agreeing with the image-domain analysis. Our calibrated data have a 5-second cadence (reduced from the 1-second cadence of the raw data), so any Arecibo-like flares should

² We note that the limit relative to bolometric quoted in McLean *et al.* (2012) is incorrect.

be apparent as several consecutive $\sim 12\sigma$ bins. We find no variability of the kind observed by RW12, with only two bins of $>3\sigma$ significance, which is consistent with the expectation from Gaussian noise of 2.6 such events.

We Hanning-smoothed the data over a variety of timescales to search for phenomena of longer duration but lower significance. Figure 2 shows the data smoothed on 30 s and 6.5 min timescales. There is a rise-and-fall pattern in the 6.5-minute cadence data suggestive of a $\sim 60\text{-}\mu\text{Jy}$ enhancement over a 20-min timescale. The data are however fully consistent with a constant flux density, matching this model with a reduced χ^2 of 1.05. We imaged a 36-minute span around the event ($56034.041 \leq \text{MJD}[\text{TT}] \leq 56034.066$) and found a source of flux density $37.2 \pm 6.8 \mu\text{Jy}$ with a background rms of $4.8 \mu\text{Jy}$, yielding a 7.8σ detection. The significance of the difference between this value and the mean flux density is lessened, however, because we searched a range of start times and durations precisely to maximize this difference. The possible flare or enhancement seen in the binned data is a factor of ~ 30 times less luminous and evolves on a timescale ~ 10 times longer than the RW12 flares. The total energy of the potential event cannot be compared to that of the RW12 flares without knowledge of its spectrum; if it is a broader-band phenomenon (see below), the two event classes could have approximately equal energies.

3. DISCUSSION AND CONCLUSIONS

Assuming that the emission from 2M 1047+21 is indeed steady and using the distance reported by Vrba et al. (2004), the radio spectral luminosity is $L_\nu = (2.2 \pm 0.7) \times 10^{12} \text{ erg s}^{-1} \text{ Hz}^{-1}$ or $\ell_{\text{rad}} - \ell_{\text{bol}} = -6.11 \pm 0.14$. We compare this value to previously-detected UCDs in Figure 3. Not only is 2M 1047+21 by far the coolest UCD to be detected in the radio, but it also has flares that are two orders of magnitude brighter than its quiescent emission, second only to the M8 dwarf DENIS J1048.0-3956 (Burgasser & Putman 2005) in the observed dynamic range of its luminosity. If the emission that we detect is not truly quiescent, the dynamic range must be even larger.

If the radio emission of 2M 1047+21 is indeed quiescent and unpolarized, it is suggestive of a gyrosynchrotron process with a brightness temperature

$$\begin{aligned} T_b &= \frac{c^2}{2k_B\nu^2} \frac{S_\nu}{\Omega} \\ &\approx (10^{6.5} \text{ K}) \left(\frac{\nu}{\text{GHz}} \right)^{-2} \left(\frac{S_\nu}{\mu\text{Jy}} \right) \left(\frac{d}{\text{pc}} \right)^2 \left(\frac{r}{R_J} \right)^{-2} \\ &\approx (10^8 \text{ K}) \left(\frac{r}{R_J} \right)^{-2}, \end{aligned} \quad (1)$$

where r is the effective radius of the emitting region and the final line plugs in the relevant values from our observation. Length scales of $r \lesssim 0.01R_J$ would be problematic for this interpretation due to the brightness temperature constraints of gyrosynchrotron emission (Dulk 1985). Gyrosynchrotron emission is broadband with a spectral peak, the location of which depends on local physical parameters. Further characterization of the radio spectrum, ideally paired with measurements in other bands, could

yield conditional estimates of the magnetic field strength and electron number density (e.g., Berger 2006).

Another candidate emission mechanism is the electron cyclotron maser instability (ECMI; Wu & Lee 1979; Treumann 2006). Stereotypical ECMI emission is highly polarized, narrowband, and time-variable, making it a natural explanation for the bursts observed by RW12. Its applicability to the emission we detect is less clear. The emission that we detect shows no evidence of strong polarization, is broadband, and may be variable but clearly does not show the strong spikes seen in 2M 1047+21 by RW12 or 2MASS J07464256+2000321 by Berger et al. (2009). Hallinan et al. (2006, 2008) have argued that continuous particle acceleration in a region of varying magnetic field strength can generate ECMI emission that is broad in frequency and time, and that propagation effects can depolarize it, potentially yielding results that are indistinguishable from gyrosynchrotron. Their arguments are partially motivated by the detection of rapid variability in the unpolarized emission of 2MASS J00361617+1821104 that would violate gyrosynchrotron brightness temperature constraints given the implied size of the emission region. If the emission we detect is really concentrated in one or possibly two weak flares of 10–20 min duration, then the same brightness-temperature argument might apply to 2M 1047+21. We note that Hallinan et al. (2008) also argue that cooler objects should tend toward more polarized emission, as propagation effects are less significant in their increasingly neutral atmospheres; if the emission we detect is strongly depolarized, it would challenge the ECMI interpretation. On the other hand, the marginal H α emission (Burgasser et al. 2003a) may suggest that the atmosphere of 2M 1047+21 may not be fully neutral.

RW12 detect three radio flares in ~ 26 hr of observing for a rate of $\sim 0.1 \text{ hr}^{-1}$. If the flares occur at random times, this is consistent with the lack of events in our 2 hr observation. It is also possible that the flares occur periodically, as observed in a significant fraction of radio-active UCDs (e.g., Berger et al. 2005, 2009; Hallinan et al. 2007, 2008), but with only three detections this hypothesis cannot be tested meaningfully. The best candidate periodicity for the three RW12 events is nominally $2.08156 \pm 0.00003 \text{ hr}$ (M. Route, priv. comm.), slightly longer than the length of time for which 2M 1047+21 is observable with Arecibo. The time baseline between the Arecibo observations and ours is sufficiently long that, even taking this periodicity and its uncertainty at face value, the phasing of our observations relative to the Arecibo flares is virtually unconstrained. We thus cannot shed any light on the regularity of the flares.

Additional observations of this unique object are clearly needed. The most pressing question to resolve is whether the quasi-quiescent emission we detect is truly steady or whether it consists of very small flares as suggested by the binned data in Figure 2. Fortunately, the sensitivity of the fully-upgraded VLA makes this a relatively straightforward proposition to test. Longer integrations allow for a more rigorous characterization of the variability of this faint source, constraining both the quasi-quiescent component as well as the duty cycle of the bright flares detected by RW12. A detection of periodicity in either of these could probe the rotation rate of 2M 1047+21, which is currently unknown. If the quasi-quiescent emission is genuinely steady, it would imply that the magnetic

field is likewise long-lived and potentially stable on a timescale of \sim years. If the quasi-quiet emission is variable, the relationship between its modulation and the temporal behavior of the RW12 flares could shed light on the magnetic field topology of 2M 1047+21.

Further observations to pin down the radio spectrum and polarization of 2M 1047+21 are also desirable. A measurement of the magnetic field strength associated with the quasi-quiet emission could be compared to the 1.7 kG estimate from the flares of RW12 to provide more clues as to the configuration of the radio-emitting regions. Strict limits on the polarization fraction would require a more careful consideration of the level of ionization in the atmosphere of 2M 1047+21 and its relation to the ECMI propagation effects proposed by Hallinan *et al.* (2008). Simultaneous multiwavelength observations (radio, $H\alpha$, optical broadband, X-rays; e.g. Berger *et al.* 2008, 2010) could probe the relationship between the photosphere, chromosphere, and corona, through monitoring of either a flare event or modulation of the quasi-quiet emission.

Both 2M 1047+21 and 2M 1315–26 (Burgasser *et al.* 2013) are exciting objects that may yield a wealth of new insights into the mechanisms of radio emission from UCDs. Both are also prime examples of the discoveries made possible by start-of-the-art, wide-bandwidth radio telescopes. The VLA in particular promises to be a key tool for the radio detection of UCDs well below the bottom of the main sequence. The tenfold increase of its sensitivity over the previous capabilities enabled the unprecedentedly low-luminosity detection presented in this Letter and will make possible the first solid constraints on the UCD radio luminosity function, successful surveys of targeted subsets of the UCD population, and detailed studies of exotic dwarfs that are rare and hence distant.

We thank Matthew Route and Aleksander Wolszczan for insight into the Arecibo results and useful discussion on the manuscript, and the anonymous referee for comments that improved the paper. We thank the NRAO for granting the Director's Discretionary Time used to make the observations presented in this Letter. We acknowledge support for this work from the National Science Foundation through Grant AST-1008361. The VLA is operated by the National Radio Astronomy Observatory, a facility of the National Science Foundation operated under cooperative agreement by Associated Universities, Inc. This research has made use of NASA's Astrophysics Data System and the SIMBAD database, operated at CDS, Strasbourg, France.

Facilities: Karl G. Jansky VLA

REFERENCES

- Benz, A. O., & Güdel, M. 1994, *A&A*, 285, 621
 Berger, E. 2002, *ApJ*, 572, 503
 —. 2006, *ApJ*, 648, 629
 Berger, E., Ball, S., Becker, K. M., *et al.* 2001, *Nature*, 410, 338
 Berger, E., Rutledge, R. E., Reid, I. N., *et al.* 2005, *ApJ*, 627, 960
 Berger, E., Gizis, J. E., Giampapa, M. S., *et al.* 2008, *ApJ*, 673, 1080
 Berger, E., Rutledge, R. E., Phan-Bao, N., *et al.* 2009, *ApJ*, 695, 310
 Berger, E., Basri, G., Fleming, T. A., *et al.* 2010, *ApJ*, 709, 332
 Browning, M. K. 2008, *ApJ*, 676, 1262
 Burgasser, A., Melis, C., Zauderer, A., & Berger, E. 2013, *ApJL*, 762, L3
 Burgasser, A., & Putman, M. 2005, *ApJ*, 626, 486
 Burgasser, A. J., Geballe, T. R., Leggett, S. K., Kirkpatrick, J. D., & Golimowski, D. A. 2006, *ApJ*, 637, 1067
 Burgasser, A. J., Kirkpatrick, J. D., Liebert, J., & Burrows, A. 2003a, *ApJ*, 594, 510
 Burgasser, A. J., Kirkpatrick, J. D., Reid, I. N., *et al.* 2003b, *ApJ*, 586, 512
 Burgasser, A. J., Sitarski, B. N., Gelino, C. R., Logsdon, S. E., & Perrin, M. D. 2011, *ApJ*, 739, 49
 Burgasser, A. J., Kirkpatrick, J. D., Brown, M. E., *et al.* 1999, *ApJL*, 522, L65
 Carson, J. C., Marengo, M., Patten, B. M., *et al.* 2011, *ApJ*, 743, 141
 Chabrier, G., & Küker, M. 2006, *A&A*, 446, 1027
 Condon, J. J. 2002, *ASP Conf. Ser.*, 278, 155
 Dobler, W., Stix, M., & Brandenburg, A. 2006, *ApJ*, 638, 336
 Donati, J. F., Morin, J., Petit, P., *et al.* 2008, *MNRAS*, 390, 545
 Dulk, G. A. 1985, *ARA&A*, 23, 169
 Durney, B. R., de Young, D. S., & Roxburgh, I. W. 1993, *Solar Physics*, 145, 207
 Fomalont, E. B., Windhorst, R. A., Kristian, J. A., & Kellerman, K. I. 1991, *AJ*, 102, 1258
 Frail, D. A., Kulkarni, S. R., Ofek, E. O., Bower, G. C., & Nakar, E. 2012, *ApJ*, 747, 70
 Gizis, J., Monet, D., Reid, N., *et al.* 2000, *AJ*, 120, 1085
 Güdel, M., & Benz, A. 1993, *ApJ*, 405, L63
 Hall, P. B. 2002, *ApJL*, 564, L89
 Hallinan, G., Antonova, A., Doyle, J. G., *et al.* 2006, *ApJ*, 653, 690
 —. 2008, *ApJ*, 684, 644
 Hallinan, G., Bourke, S., Lane, C., *et al.* 2007, *ApJL*, 663, L25
 McLean, M., Berger, E., & Reiners, A. 2012, *ApJ*, 746, 23
 McMullin, J. P., Waters, B., Schiebel, D., Young, W., & Golap, K. 2007, *ASP Conf. Ser.*, 376, 127
 Mohanty, S., Basri, G., Shu, F., Allard, F., & Chabrier, G. 2002, *ApJ*, 571, 469
 Morin, J., Donati, J. F., Petit, P., *et al.* 2008, *MNRAS*, 390, 567
 Reiners, A., & Basri, G. 2006, *ApJ*, 644, 497
 —. 2007, *ApJ*, 656, 1121
 Route, M., & Wolszczan, A. 2012, *ApJL*, 747, L22
 Rutledge, R. E., Basri, G., Martín, E. L., & Bildsten, L. 2000, *ApJL*, 538, L141
 Sault, R. J., & Wieringa, M. H. 1994, *A&AS*, 108, 585
 Semel, M. 1989, *A&A*, 225, 456
 Stelzer, B., Micela, G., Flaccomio, E., Neuhäuser, R., & Jayawardhana, R. 2006, *A&A*, 448, 293
 Treumann, R. 2006, *A&A Rev.*, 13, 229
 Vrba, F. J., Henden, A. A., Luginbuhl, C. B., *et al.* 2004, *AJ*, 127, 2948
 West, A. A., Hawley, S. L., Walkowicz, L. M., *et al.* 2004, *AJ*, 128, 426
 Wu, C. S., & Lee, L. C. 1979, *ApJ*, 230, 621

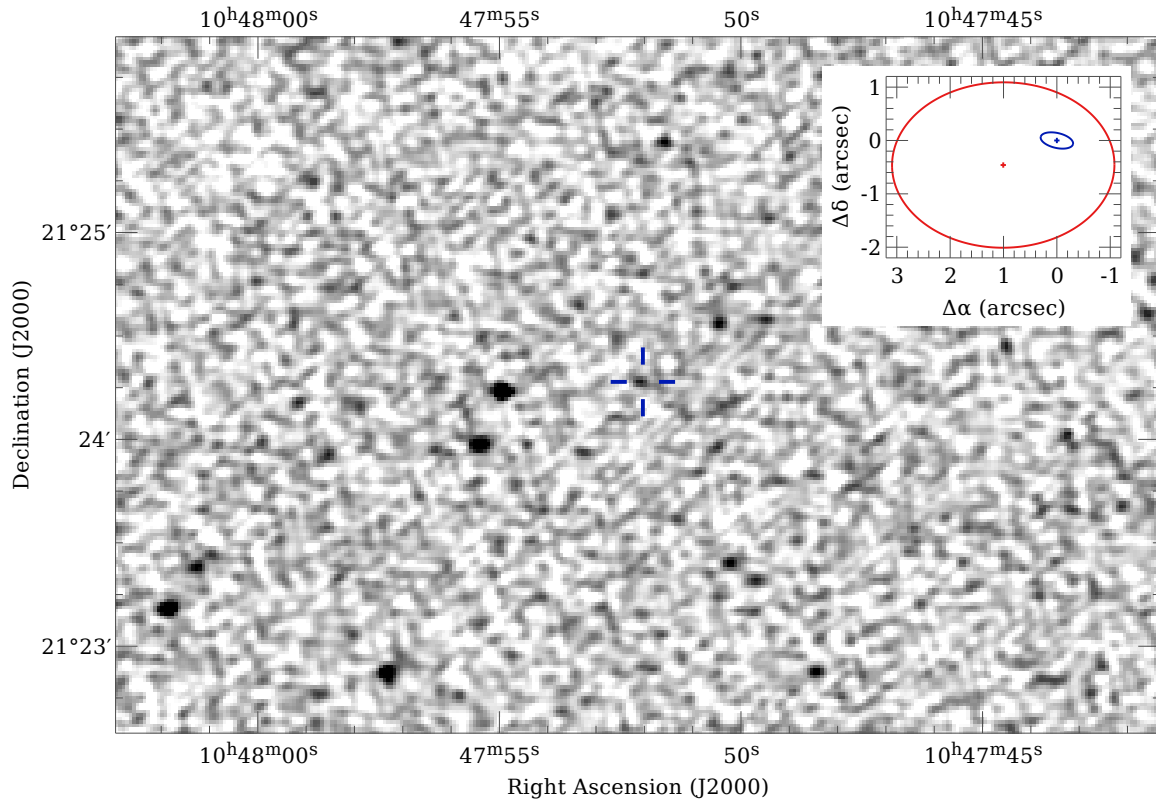


Figure 1. VLA detection of 2M 1047+21. The grayscale is linear black-to-white from -5 to +20 μJy . The background rms is 3.6 μJy . The crosshairs in the main image are centered on the predicted location of 2M 1047+21 from Vrba et al. (2004), which is independent of our radio observations. The enlarged inset compares the 1σ confidence regions of the VLA (red ellipse) and Vrba et al. (2004, blue ellipse) positions.

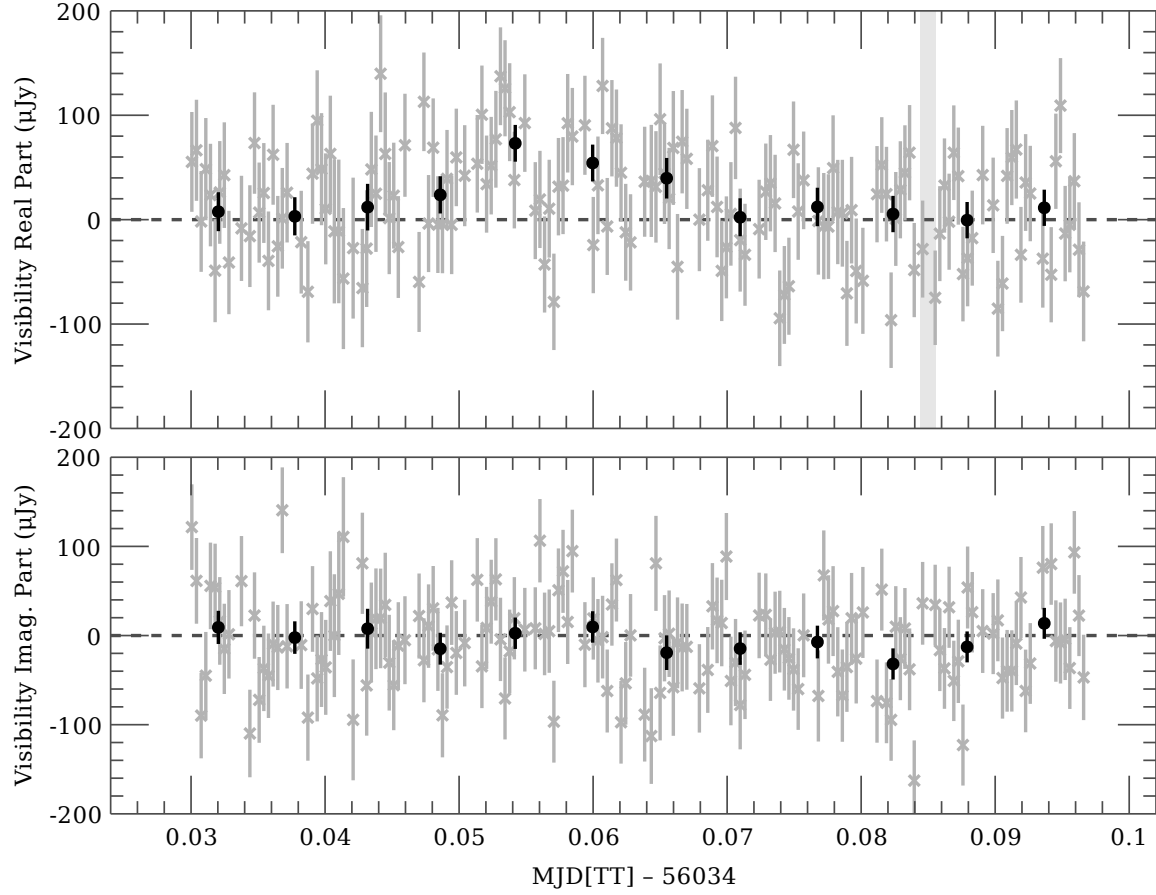


Figure 2. Visibility-domain photometry of 2M 1047+21 as described in §2. *Upper panel:* the real parts of the summed visibilities, giving the nominal source flux density. *Lower panel:* the imaginary parts, which would be zero if there were no noise or calibration errors. *Light axes:* the summed visibilities after Hanning smoothing on a 1-minute timescale and decimating by a factor of 6, yielding a 30-second cadence in which adjacent measurements are weakly correlated. *Dark circles:* the summed visibilities smoothed on a 6.5-minute timescale and decimated by a factor of 78, so that adjacent measurements are uncorrelated. The light curve is suggestive of variability with a timescale of ~ 0.5 hr and a peak flux density of $\sim 60 \mu\text{Jy}$. The width of the *shaded band* is 100 s, the timescale of the flares detected by RW12; its horizontal position is arbitrary. At flux densities of ~ 2 mJy, such flares would register as $\sim 12\sigma$ bins in our 5-second-cadence data (approximately accounting for the flare rise and fall) or \sim two 30σ bins in the 30-second-cadence data plotted here.

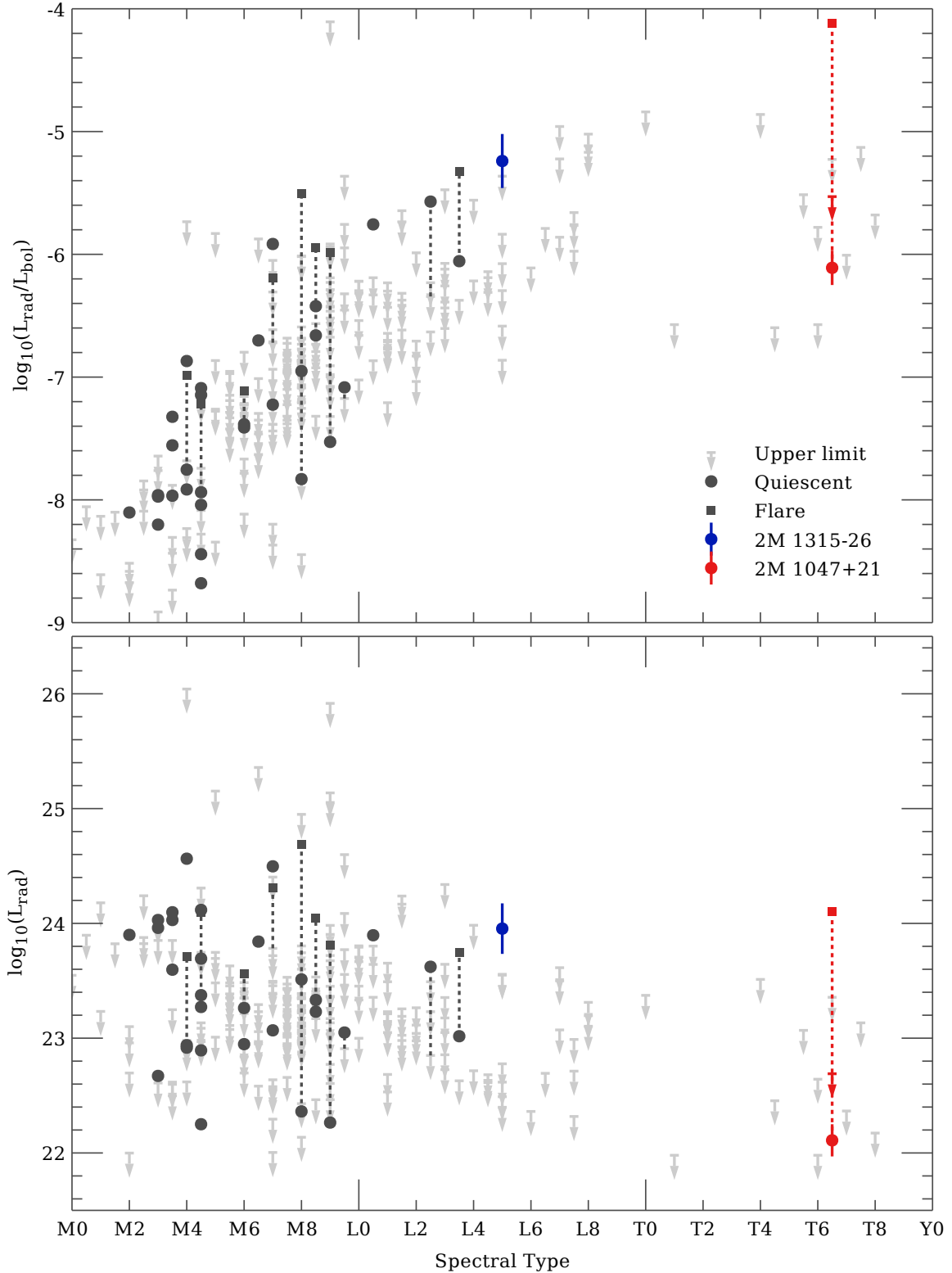


Figure 3. Ultracool dwarf radio luminosity as a function of spectral type. *Upper panel:* normalized to the bolometric luminosity. *Lower panel:* unnormalized. The background data are from McLean et al. (2012, and references therein). The measurement of 2M 1315–26 by Burgasser et al. (2013) is in blue. Recent measurements of 2M 1047+21 are in red (flare: RW12, upper limit: Berger (2006), quiescent: this work, assuming steady emission). It is the only radio-detected ultracool dwarf of spectral type T, and its flares as detected by RW12 are an order of magnitude more luminous, relative to L_{bol} , than those from other UCDs. Our detection is the lowest-luminosity yet achieved for a UCD.